Compressed ion temperature gradient turbulence in diverted tokamak edge[a)]

C. S. Chang,[1,2,b)] S. Ku,[1] P. H. Diamond,[3] Z. Lin,[4] S. Parker,[5] T. S. Hahm,[6] and N. Samatova[7]
[1]*Courant Institute of Mathematical Sciences, New York University, New York, New York 10012, USA*
[2]*Department of Physics, Korea Advanced Institute of Science and Technology, Daejon 305-701, Republic of Korea*
[3]*Center for Astrophysics and Space Sciences and Department of Physics, University of California, San Diego, La Jolla, California 92093, USA*
[4]*Department of Physics and Astronomy, University of California, Irvine, California 92697, USA*
[5]*University of Colorado at Boulder, Boulder, Colorado 80309, USA*
[6]*Princeton Plasma Physics Laboratory, Princeton, New Jersey 08543, USA*
[7]*North Carolina State University, Raleigh, North Carolina 27695, USA and Oak Ridge National Laboratory, Oak Ridge, Tennessee 37831, USA*

(Received 7 December 2008; accepted 23 February 2009; published online 3 April 2009)

It is found from a heat-flux-driven full-f gyrokinetic particle simulation that there is ion temperature gradient (ITG) turbulence across an entire L-mode-like edge density pedestal in a diverted tokamak plasma in which the ion temperature gradient is mild without a pedestal structure, hence the normalized ion temperature gradient parameter $\eta_i=(d \log T_i/dr)/(d \log n/dr)$ varies strongly from high (>4 at density pedestal top/shoulder) to low (<2 in the density slope) values. Variation of density and η_i is in the same scale as the turbulence correlation length, compressing the turbulence in the density slope region. The resulting ion thermal flux is on the order of experimentally inferred values. The present study strongly suggests that a localized estimate of the ITG-driven χ_i will not be valid due to the nonlocal dynamics of the compressed turbulence in an L-mode-type density slope. While the thermal transport and the temperature profile saturate quickly, the $E\times B$ rotation shows a longer time damping during the turbulence. In addition, a radially in-out mean potential variation is observed. © *2009 American Institute of Physics*. [DOI: 10.1063/1.3099329]

I. INTRODUCTION

Plasma transport in the edge region is an important research area critical to the success of the toroidal magnetic fusion program. Together with the neutral transport, the heat out-flux from the core, and the edge localized mode instability, the edge transport determines the edge pedestal shape and height, which then strongly influences the fusion yield in the core plasma by determining a boundary condition. It is predicted that ITER (Ref. 1) requires a certain level of self-organized edge pedestal height in order to achieve its goal $Q=10$ (ratio of output energy to input energy). Spontaneous development of the high edge pedestal requires transport transition into H-mode[2] in the same general edge area (H-layer) just inside the magnetic separatrix. The H-mode transition cannot be understood unless the plasma transport is understood in the L-mode edge prior to the transition.

Even in an L-mode plasma, there is usually a steep density slope localized to the edge (we call it "edge density pedestal" in the loose sense). The edge density pedestal in L-mode is normally lower in height and wider in radial width than the density pedestal in H-mode. On the contrary, the radial edge temperature gradient in L-mode stays globally gradual without a distinctive edge pedestal structure until after the H-mode transition occurs. This leads to low η_i ($\equiv \partial_r \log T_i/\partial_r \log n=$density gradient scale length/ion temperature gradient scale length) in the L-mode edge density slope except at the top, making it difficult for the pure ion temperature gradient (ITG) driven mode to be linearly unstable according to a local theory. Thus, in a conventional reduced transport modeling, the pure ITG has been assumed to be absent in the L-mode density pedestal slope, leaving the ion transport to other types of turbulence. On the other hand, the value of η_i can be large (and rapidly varying radially) at the density pedestal top/shoulder where the density gradient scale length is long. In the present work, we study an "L-mode-like" edge plasma which possesses these properties, i.e., a wide density pedestal and a mild ion temperature gradient without an H-mode-like pedestal structure.

The ITG modes usually exhibit a robust turbulence activity which may dominate the edge transport if it is unstable, with the wavelength of significant modes stretching to the level of the L-mode edge gradient scale length. A nonlocal edge gyrokinetic simulation over a widely varying η_i, whose radial scale length is similar to the radial turbulence correlation length, is needed for a more reliable prediction of the plasma transport and the self-organized η_i profile relaxation. Existence of the ITG turbulence could also significantly influence the characteristics of other possible turbulence activities in the L-mode edge.

Study of ITG turbulence around the H-layer has been difficult for a few reasons. The first reason is the existence of

[a)]Paper NI1 5, Bull. Am. Phys. Soc. **53**, 160 (2008).
[b)]Invited speaker. Electronic mail: cschang@cims.nyu.edu.

magnetic separatrix geometry including X-point, which makes the guiding center equation of motion in a flux-coordinate system to suffer from a mathematical singularity (the magnetic rotational transform vanishes at the separatrix) in ordinary gyrokinetic codes developed for efficient study of core turbulence physics. The second reason is the nonseparability of the radial scale length between the equilibrium gradients ($L_\perp$) and the ITG mode fluctuations (Δ_{turb}) as alluded in the previous paragraphs. In the usual case, the four scale characteristics of ITG zonal flow turbulence, namely, $L_\perp$—the plasma gradient scale length, L_E—the fluctuation envelope and thus the zonal flow scale, Δ_{turb}—the turbulence correlation length, and ρ_i the ion gyroradius, are well separated. Indeed, usually $\rho_i < \Delta_{\text{turb}} < L_E < L_\perp$. For compressed turbulence, as encountered here and to be detailed later in the edge density slope, we have $\rho_i < \Delta_{\text{turb}} \sim L_E \sim L_\perp$. This can allow strong nonlinear interaction between the turbulence and the mean equilibrium. This invalidates the mixing length argument and the local diffusion ansatz. In particular, note that conventional mixing length estimates, dating back to L. Prandtl, are based on the idea that the fluctuation δf is due to the Δ-scale rearrangement of mean $\langle f \rangle$

$$\delta f(r) \simeq \langle f(r+\delta r)\rangle - \langle f(r)\rangle \simeq \Delta r\, \partial\langle f\rangle/\partial r,$$

leading to $\delta f/\langle f\rangle \simeq \Delta r/L_\perp$. This expansion is firmly rooted in the ordering $\Delta r \ll L_\perp$. Then, in this ordering,

$$\langle(\delta f)^2\rangle \simeq \langle \Delta r^2\rangle(\partial\langle f\rangle/\partial r)^2 \simeq D_r \tau_c (\partial\langle f\rangle/\partial r)^2,$$

where $D_r \simeq \Delta r^2/\tau_c$. Equivalently, both validity of mixing length theory and validity of δf expansion rest upon the condition that a phase density element traverses a scale length $L_\perp$ by means of a multistep random walk. However, in compressed edge turbulence, $\Delta r \sim L_\perp$. Thus, the first order truncation of the expansion in $\Delta r/L_\perp$ is invalid.

The third reason for the difficulty is the coexistence of the open and the closed field line regions in the edge. A conventional delta-f method is not suitable for handling the open field line region since the assumption of a fixed background distribution function f_0 and the condition of phase space conservation are invalid due to loss of particles to the wall. The conventional delta-f simulations, which have been developed for economical core plasma turbulence simulation, assumes fixed background equilibrium and studies the perturbed part only, hence cannot address the problems associated with the second and third difficulties in the edge plasma.

In the present work, we use a special full-function (full-f) gyrokinetic code XGC1 (see Sec. II and Refs. 3 and 4) to study ITG turbulence across the magnetic separatrix in divertor geometry. Neoclassical and turbulent plasma dynamics are simulated together self-consistently, with their radial scale lengths being similar to each other in an L-mode type of edge plasma in DIII-D geometry.[5] Unlike in a delta-f kinetic simulation, a full-function simulation deals with the whole equation $df/dt = S$, where S represents sources and sinks, and does not require the phase volume conservation $df/dt = 0$ (see Ref. 6, and references therein). Thus, a full-f simulation is a necessity to handle the edge plasma. We note here that there are other full-f gyrokinetic codes under development for core plasma studies.[7–9]

The rest of this paper is organized as follows. In Sec. II, a brief description of the full-f XGC1 gyrokinetic code is presented. In Sec. III, the full-f simulation concept is emphasized in more detail for plasma edge simulation. In Sec. IV, the simulation conditions and the simulation results are described. In Sec. V, conclusion and discussion are presented.

II. THE XGC1 FULL-*F* GYROKINETIC CODE

XGC1 is a full-f gyrokinetic particle-in-cell code, which can include the magnetic separatrix and the biased material wall.[3,4,10,11] In the present study, we use full-f marker particles for neoclassical/turbulent ions and neoclassical electrons. Adiabatic electrons are used for the ITG turbulence response. We simulate the neoclassical and the turbulence physics together self-consistently so that the pedestal plasma can evolve into self-organized radial profiles.

The following Lagrangian guiding center equation of motion is advanced in cylindrical coordinate system instead of the conventional flux-coordinate system, in order to avoid the singularity problem toward the magnetic separatrix surface, while conserving the mass, canonical angular momentum, and energy:[12]

$$\dot{\mathbf{X}} = (1/D)[u\hat{b} + (u^2/B)\,\nabla B \times \hat{b} + \{\mathbf{B} \times (\mu \nabla B - \mathbf{E})\}/B^2],$$

$$\dot{u} = -(1/D)(\mathbf{B} + u\,\nabla B \times \hat{b}) \cdot (\mu \nabla B - \mathbf{E}), \tag{1}$$

$$D = 1 + (u/B)\hat{b} \cdot (\nabla \times \hat{b}),$$

where u is the parallel speed of the particle to the local magnetic field vector $\mathbf{B}$, $\hat{b} = \mathbf{B}/B$, μ is the magnetic moment, and $\mathbf{E}$ is the gyroaveraged electric field. In order to take advantage of the slowly varying nature of the electric potential (both neoclassical and turbulent) along the magnetic field lines, the particle push uses u and μ velocities and the electrostatic potential is solved on an approximately field line following mesh. The following gyrokinetic-Poisson equation[13] is solved on the mesh with the four-point averaging technique:[14]

$$-\nabla_\perp \frac{\rho_i^2}{\lambda_{Di}^2} \nabla_\perp \Phi = e(1 - \nabla_\perp \rho_i^2 \nabla_\perp)(\bar{n}_i - n_e), \tag{2}$$

where ρ is the gyroradius vector and λ_{Di} is the ion Debye length. $\bar{n}_i$ is the numerically evaluated ion density which includes the second derivative of the equilibrium density and temperature,[6]

$$\bar{n}_i = \frac{1}{2\pi}\int f_i(\mathbf{X}, \mu, u)\, \delta(\mathbf{X} - \mathbf{x} + \boldsymbol{\rho}_\mathbf{i})\, d\mathbf{X} d\mu du d\alpha,$$

where $\mathbf{x}$ is the real particle position vector, $\boldsymbol{\rho}_\mathbf{i}$ is gyroradius vector, and α is the gyrophase. The above gyrokinetic-Poisson equations are valid for the plasma gradient scale length much greater than the ion gyroradius ρ_i, which is satisfied in the H-mode edge in conventional tokamaks where the steep pedestal width is on the order poloidal gyroradius $\gg \rho_i$. Specifically in the present simulation, mimicking a high

temperature DIII-D *L*-mode density pedestal before the *H*-mode transition, with an average temperature in the density pedestal slope of ~400 eV and the magnetic field strength $B \sim 2.1$ T, the deuteron gyroradius is ~1.4 mm (nominal $\rho_* \equiv a/\rho_i = 429$ for $a = 60$ cm). Thus, the validity of the equations requires that the radial density scale length to be $\gg 1.4$ mm. The radial density scale length 40 mm used in the present simulation satisfies this validity limit. Since the neoclassical particle transport is negligibly small and the electrons react to the turbulence adiabatically, the density gradient scale length remains unchanged through out the simulation. We note here that the potential term on the left-hand side of Eq. (2) (on the order $\rho_i^2/L_\perp^2$) is not weaker than the neoclassical drive from magnetic inhomogeneity (on the order ρ_i/R) in the term $\overline{n_i} - n_e$ on the right-hand side. Thus, the electrostatic potential is completely determined in the edge plasma. Another consequence is that the mesoscale turbulence can be more tightly coupled to the neoclassical physics, which is a property of the edge compressed turbulence.

The boundary condition on the Poisson equation is that the electrostatic potential at the outer boundary (material wall) is grounded ($\Phi = 0$), and the mean E_r and $\delta\Phi$ at the inner boundary vanishes. The gradients in particle number density and temperature at the inner boundary are chosen to be small. Magnitude of the particle number density and the temperature are not fixed in time at the boundaries. They are free to change according to the transport, source, and sink. At the outer boundary, when the particles hit the wall, they are lost (absorbing boundary). At the radially inner boundary, however, the particles come back following the collisionless guiding center orbits (reflection boundary with proper reflection orbits). We put a specified rate of heat source around the radially inner boundary for heat flux from the core plasma. Heating is achieved by increasing the particle energy at the inner boundary at a uniform rate while keeping the particle pitch angle fixed. We use an artificially elevated level of ion-ion collisions in the inner boundary to force the plasma to accept some heat flux into the turbulence region from the heating region. Without this artificial collisional heat transport, we find that the plasma can self-organize to reject the radial heat flux from the source region.

XGC1 uses a realistic numerical magnetic equilibrium from a g-eqdsk data file.[15] A particle, momentum and energy conserving linear Monte Carlo Coulomb collision operation is built into the particle motion (see Ref. 16, and references cited therein). In order to handle the *X*-point geometry and the odd-shaped material wall, the computational mesh used in XGC1 is unstructured triangular in the radial-poloidal plane, but still regular in the toroidal direction. A typical computational mesh in XGC1 for ITG turbulence studies in a DIII-D size tokamak edge consists of ~16–64 toroidal, 80 radial and ~1000 poloidal grid points. Convergence study shows that 16 toroidal grids in the whole toroidal angle ($0-2\pi$ radians) yields adequately converged ion heat flux. The number of radial and poloidal grid points has been decided after a convergence study, too, and the grid distance is about one ion gyroradius on the average. As usual, the number of toroidal grid points are much less than the number of radial/poloidal grid points due to smallness of $k_\parallel/k_\perp$ in a field line following Poisson solver system, which is further reduced by the large safety factor q in the edge region. Monte Carlo neutral particles can also be simulated together in the XGC family codes.[10] In the present work, however, the neutral particle routine is not used.

III. PROPERTIES OF A FULL-*F* PARTICLE SIMULATION

Full-function kinetic simulations solve the full gyrokinetic Fokker–Planck equation $df/dt = C(f) + S$, where C is the collision operator and S is the source/sink operator. Major advantages in a full-*f* simulation (in comparison with the conventional delta-*f* simulation) are in the ability to calculate the mean and the perturbed parts of the plasma together, in the facilitation of sources and sinks, in the natural inclusion of more complete physics such as the velocity space nonlinearity [contained in the $\vec{E}$ force in the parallel velocity acceleration equation (1)], and in the nongrowth of the marker particle weights. In return, the particle simulation is expensive: a full-*f* gyrokinetic particle-in-cell code requires much more marker particles than a delta-*f* gyrokinetic code. Fortunately, the simulation can be carried out for a long time (longer than a collision time) without suffering from the growth of the particle weights as in a delta-*f* code. A delta-*f* code requires more number of particles for a long time simulation than a short time simulation due to the growing weight issue. Thus, the required particle number ratio between a full-*f* simulation and a delta-*f* simulation is less than what is deduced from a simple $\sqrt{N}$ argument. The actual number of full-*f* marker particles used in this study will be discussed in Sec. IV.

Ability to handle the mean plasma dynamics is an important advantage of a full-*f* simulation, as described earlier. This capability enables a full-*f* simulation to study the self-organized "stiffness" nature of plasma profiles. In the present study, the mean part of the plasma is classified into two categories according to the physics drives. The first category belongs to the well-known neoclassical plasma equilibrium with Coulomb collisions. The classical drive (from the finite gyro excursion effect) is usually much smaller than the neoclassical drive (from the finite guiding center excursion effect) in a conventional toroidal confinement system except for the classical sheath phenomenon in front of a material boundary. For convenience, we include the sheath phenomenon into the "neoclassical" category.

The second category corresponds to the turbulence-driven mean plasma. Turbulence-driven mean plasma can interact with the turbulence in a similar way as the neoclassical mean plasma can. As a matter of fact, the gyrokinetic equation automatically satisfies the fluid moment equations, including the radial force balance equation, and an experimental distinction between the neoclassical-driven and the turbulence-driven mean plasma is not trivial. In a numerical simulation, the turbulence-driven mean plasma dynamics disappears as the turbulence is turned off, even though the turbulence might have modified the semi-indeterminate part (i.e., toroidal rotation) of the plasma profiles.

Since the flow shearing physics is of special interest in understanding the turbulence dynamics, we describe here a simple criterion in distinguishing the turbulence-driven mean flows from the zonal flows as used in the present work. Both the turbulence-driven "mean" and "zonal" electric field $\tilde{E}_r$ and $\tilde{E}_r \times B$ flows are the flux-surface and toroidally averaged quantities. Turbulence-driven mean flows can vary as slowly as the neoclassically driven mean flow in the ion-ion collision time (τ_{ic}) scale, hence can interact with turbulence eddies in the same manner as the neoclassical flows do. A turbulence-driven mean flow component with a much slower variation than τ_{ic} will be damped by the ion-ion collisional neoclassical mechanism. For this reason, the scale separation boundary between the turbulence-driven mean and zonal flows is set at τ_{ic} in the present work. In other words, mean flows with oscillation frequency faster than $\nu_i = 1/\tau_{ic}$ is identified as zonal flows. In the plasma studied here, the representative ion-ion collision time in the middle of the density slope is $\nu_{ic} \simeq 2$ kHz (actually, the collisionality varies from banana regime at the density pedestal top to plateau regime in the slope), which is much below the geodesic acoustic mode (GAM) frequency ~40 kHz (as observed in the simulation, which is similar to v_i/R, where v_i is a representative ion thermal speed and R is the major radius of torus). Hence, there is a wide window of zonal flow frequencies. It will be shown in Sec. IV that, unlike in a core plasma, the diamagnetic frequency in the edge density pedestal is higher than the GAM frequency. The radial correlation extent of the zonal and GAM oscillations are "mesoscale," as is well known, in between the device size and the ion gyroradius.[17] Radial variation scale length of the turbulence-driven "mean" plasma profiles appearing in a full-f simulation is similar to the neoclassical scale, or the radial turbulence energy envelope scale, whichever is smaller. In the edge plasma, all these radial scales are similar to each other, as discussed earlier.

In the steep edge plasma around the magnetic separatrix, there is no accurate analytic neoclassical theory which enables extraction of the neoclassical mean flow from the turbulence combined mean flow. In the simulation, however, a collisional neoclassical phenomenon establishes quasiequilibrium pressure, flow, and E_r profiles (strictly speaking, only their relations in the far core side plasma where the edge effect is weaker) in the edge before the turbulence develops. In a broad sense, any change in the mean profiles by turbulence can be regarded as the turbulence-driven modification, which can be recovered if we turn off the turbulence as long as the unrecoverable part (i.e., the toroidal flow) is small. In a narrow sense, however, the change of plasma temperature gradient by turbulence could lead to the change in the neoclassical part of E_r and toroidal flow (plasma density profile does not change in an adiabatic simulation). Our previous simulations, in agreement with the core neoclassical theories, show that the neoclassical E_r and the toroidal/parallel flow are sensitive to the density gradient, and relatively insensitive to the temperature gradient in the banana-plateau regimes. If the temperature profile saturates to a self-organized state and experiences an insignificant change during the longer time nonlinear plateau phase of turbulence, a significant change in the mean $E \times B$ flows can only be turbulence driven in the absence of the density gradient change. This is an interesting subject and deserves a separate publication after a systematic study in the future. The results to be presented here is preliminary.

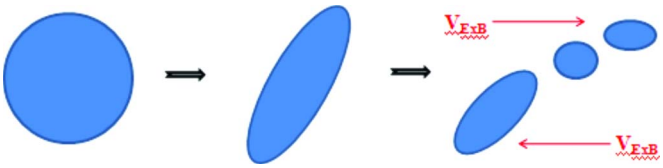

FIG. 1. (Color online) Cartoon illustration of a large scale eddy being sheared into small scale turbulence (see Ref. 18).

Distinction between the mean physics and the zonal flow/field physics is necessary from the turbulence physics point of view, in addition to the equilibrium physics point of view. As is well discussed in literature (see, for example, the review article by Diamond *et al.*[17]), a mean $E \times B$ flow shearing plays a different role from a zonal $E \times B$ shearing in the generation of small scale turbulence from large scale eddies (see Fig. 1, credited to Ref. 18). Mean $E \times B$ shearing, usually on the $L_\perp$ scale, increases k_r according to $k_r = k_{r0} - k_\theta \langle V_{E\times B} \rangle' t$. Thus, $\langle \delta k_r^2 \rangle \sim k_\theta^2 \langle V_{E\times B} \rangle'^2 t^2$ and k_r grows ballistically. Zonal shearing, however, drives random walk in k_r. Thus $k_r^2 \sim D_{rk} \langle V'^2_{E\times B} \rangle \tau_{c,ZF} t$, where $\tau_{c,ZF}$ is the zonal flow correlation time.[17] Repartion of energy between the mean and the zonal flows can allow for a higher level of turbulence than when only considering zonal flows. Moreover, since mean flows can be driven by both heating/fueling (via ∇P) and turbulence, while zonal flows are exclusively turbulence-driven, nontrivial energy exchange cycles are possible involving the interplay of zonal and mean flows.[19] Even when the turbulence interaction with the mean $E \times B$ shearing is weaker than its interaction with the zonal $E \times B$ shearing, the long time contribution to turbulence from mean $E \times B$ shearing could be significant. Breaking the large scale eddies into small scale turbulence by shearing usually results in the quench of the turbulence drive process and the reduction of plasma transport.

IV. FULL-*F* SIMULATION OF RADIALLY COMPRESSED ITG TURBULENCE IN AN *L*-MODE LIKE EDGE DENSITY SLOPE

We start this section with a simple dispersion relation for the ITG modes[20,21]

$$\omega_{n*}/\omega - 2\omega_d/\omega - 7\omega_d^2/\omega^2 + 2\omega_d\omega_{n*}(1+\eta)/\omega^2 + K = 0,$$

where $\omega_{n*} = k_\theta \rho_i / L_n$, $\omega_d = k_\theta \rho_i / R$, $K = T_i/T_e$, L_n is the density gradient scale length and R is the major radius of the torus. In the limit of strong density gradient, the dispersion relation is reduced to the solution

$$\omega = [-\omega_{n*} \pm \sqrt{\omega_{n*}^2 - 8K\omega_d\omega_{n*}(1+\eta)}]/(2K).$$

Thus, ITG is unstable if $\eta_i > \eta_c = (R/8KL_n) - 1$. In a DIII-D edge plasma modeled in the present work, this relation leads to $\eta_c = 4.4$ for $R = 173$ cm, $K = T_i/T_e = 1$, $L_n = 4$ cm and

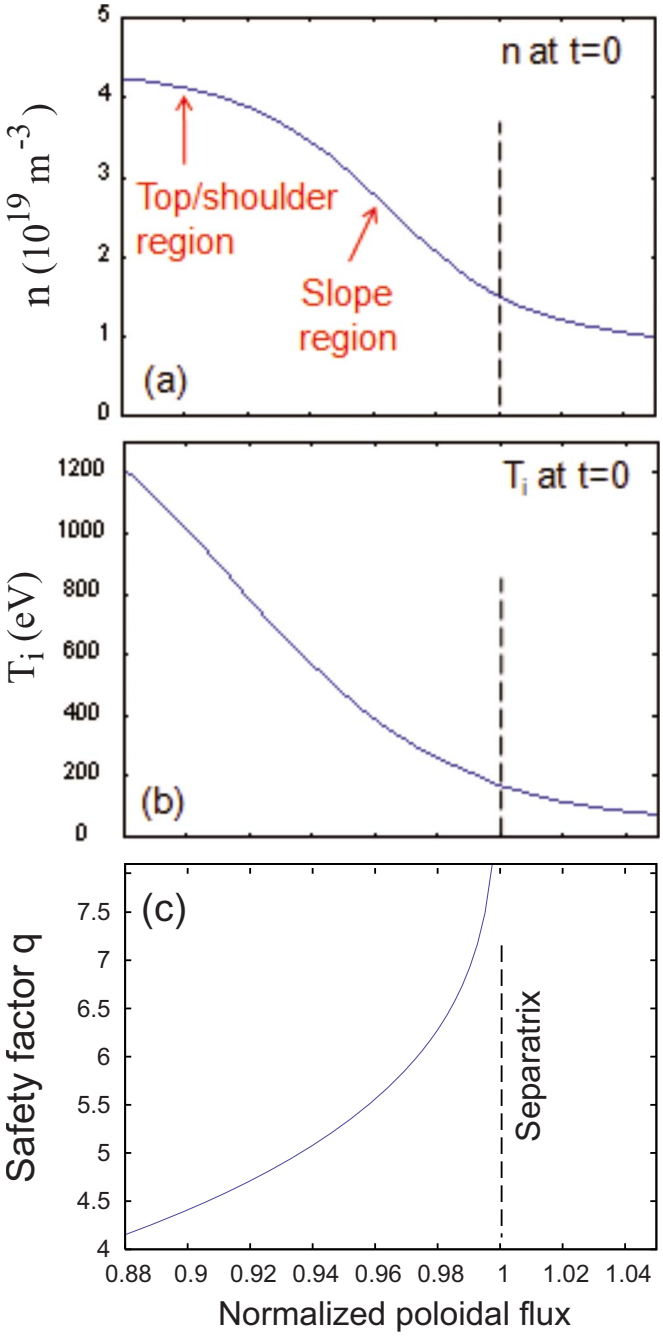

FIG. 2. (Color online) Initial density (a) and temperature (b) profiles, and the safety-factor q profile (c).

$R/L_n=43.3$. Even though there is no guarantee that this idealized estimate is accurate for a plasma around the magnetic separatrix, we will use this common estimate as the guideline for the linear stability of ITG modes in the present work.

As explained earlier, experiments usually find a density pedestal in a diverted L-mode tokamak edge, while the radial edge temperature gradient is mild without a distinctive pedestal shape. Thus, the η_i value in the L-mode density pedestal slope is usually small ($\eta_i \leq 2$), leading to a local estimate that the pure ITG mode is stable. In the present simulation, we mimic this experimental situation by using a moderate density pedestal and a much milder temperature profile in the form of hyperbolic tangent (see Fig. 2). In Fig. 2, profile of

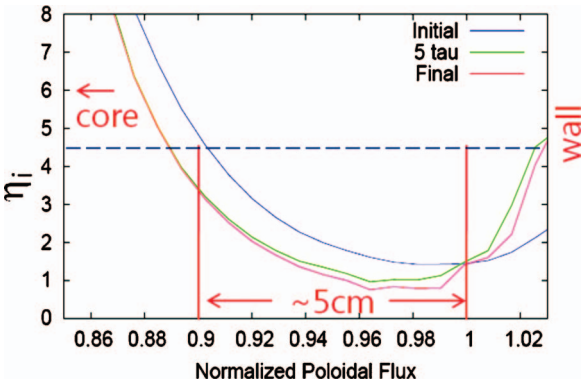

FIG. 3. (Color) η_i profiles at the initial time (blue), after the thermal transport settles down (green) and at the finish of simulation (red).

the safety factor q is from the experimental data file. The electron temperature is assumed to be equal to the ion temperature. The initial η_i profile is shown in Fig. 3 in blue color. Figure 4 shows the radial distribution of $\omega_{n*}/2\pi$, which is, as expected, much higher than the usual values found in the core plasma.

The conventional units used in the core plasma simulation are not convenient in the edge where the radial scale length is unconventionally small. In the present work, due to the importance of the ion orbital behaviors in a full-f simulation, we use the ion toroidal transit time τ_{it} as the basic time unit. For a perfectively passing ion with the temperature of 400 eV in the middle of density slope and the major radius on the magnetic axis of 173 cm in DIII-D, we have $\tau_{it}=0.078$ ms. For an easier comparison with the experiments, the diffusion rate is also given in the real unit m^2/s. To help the readers who are familiar with the core gyrokinetic turbulence results, we present the conversion table in Fig. 5.

In a full-f simulation, reaching a quasisteady self-organized equilibrium from the particle loading is the first step in the Fokker–Planck Poisson system. The initial particle loading can be achieved in two different ways. The first method is to use the canonical Maxwellian distribution (nonlocal Maxwellian).[22,23] Even though this initialization method has the advantage of a rapid self-organization to a quasisteady equilibrium without spurious drive of GAM

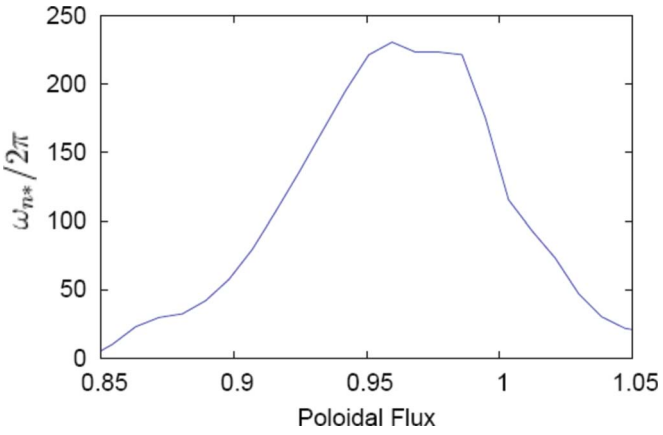

FIG. 4. (Color online) Radial distribution of $\omega_{n*}/2\pi$.

Physical quantity	Value	Conversion factor
Ion thermal speed (T=400eV, Deuteron)	$v_i=(kT/m)^{1/2}$ $=1.4\times10^7$ cm/s	
Toroidal transit time τ_{it} (R_{axis}=173cm, a=60cm)	$2\pi R/v_i$ $=7.8\times10^{-2}$ ms	$\tau_{it}=1.3\times10^3$ gyro time $=18.2\ a/v_i$
Ion collision time τ_{ic} ($n=3\times10^{13}$ cm^{-3})	4.6×10^{-1} ms	$\tau_{ic}=5.9\ \tau_{it}$
Ion gyro radius ρ_i (B=2.1 T)	0.14 cm	
D (Global Gyro-Bohm)	$D_{GB}=\rho_i T/aeB$ $=0.44$ m^2/s	

FIG. 5. Conversion table from the ion toroidal transit time to conventional gyrokinetic time units in DIII-D edge plasma used in the simulation. Comparison of real unit length and diffusion coefficient to gyroradius and gyro-Bohm (global) is shown together.

modes, we find that it is not well suited for an edge pedestal simulation due to difficulty in the density and temperature profile control.

The second method is to load the particles initially as local Maxwellian, with flux-function density and temperature profiles. This method has a disadvantage in that it consumes a longer computing time before the system self-organizes to a quasisteady equilibrium after a large disturbance by different radial excursions between the ions and electrons. It has been known that this initial disturbance could lead to spurious GAM oscillations and zonal/parallel parallel flow generation which can quench turbulence,[23,24] or to a delayed occurrence of turbulence if a flux-driven boundary condition is used.[25] A proper quiet start technique and/or a flux drive is necessary. The local Maxwellian loading also contains some unspecified canonical toroidal rotation, which is, fortunately, insignificant compared to the thermal speed v_i in the present simulation. A considerable advantage in the local Maxwellian loading is the easy control of the initial density and temperature profiles. Since the control of the plasma profile is a critical feature in the edge turbulence study, we take this approach in the present study. In order to minimize the possibility of strong spurious GAM and zonal flows in the turbulence stage from the initial Maxwellian loading, we obtain an approximate axisymmetric quasineoclassical solution in a separate preconditioning simulation and use it as the initial condition to the full-f turbulence simulation. This technique serves as the primary quiet start procedure in the turbulence simulation. We find that even an approximate neoclassical solution can serve the purpose.

The initial steady-state solution is obtained from the full-f gyrokinetic ions and full-f drift kinetic electrons in the axisymmetric mode by filtering out the electric field perturbations before the ion and electron push operations at each time step.[3] The parallel Debye sheath, which is a small scale subgrid phenomenon and not resolved in a gyrokinetic simulation, is forced to be included in the large scale presheath for quasineutrality and ambipolarity.[3] Detailed information on obtaining the edge equilibrium solution can be found in Ref. 3.

A turbulence simulation, unlike the initial axisymmetric simulation, is then performed using the adiabatic electron response starting from the self-organized axisymmetric equilibrium as the initial condition. As a method for a secondary quite start, we run the marker ions first in the real geometry to obtain the neoclassical orbital spread. We then put the marker electrons on top of each marker ions. If there is any need for an adjustment from the approximate initial axisymmetric electric field, the system finds the adjustment within one ion toroidal transit time τ_{it}. We note here that the GAM oscillations in the edge plasma can easily be excited and sustained due to largeness in the safety factor q. The present procedure removes strong spurious growth of GAMs and gives protection from turbulence quench, but some GAMs are still generated and survived during the edge turbulence simulation, as will be shown later. The more exact the initial condition is, the weaker the initial GAM perturbations will be.

For further simplification of the turbulence simulation in the scrape-off region, it is assumed that the electrical connection of the open magnetic field lines to the conducting wall does not allow the turbulence modification of the poloidally averaged axisymmetric part of the electric potential $\Phi_{0,0}$ (the toroidal mode number n and the poloidal mode number m are both 0) in the scrape-off region. This puts a limitation on the turbulence modification capability of the plasma potential $\Phi_{0,0}$ relative to the grounded wall in the scrape-off region. Inside the magnetic separatrix, however, we allow $\Phi_{0,0}$ to evolve freely by the turbulence effects, together with the zonal fluctuations and GAM oscillations. Another limitation to the present simulation is the use of adiabatic electron response to turbulence. Particle transport by turbulence is, thus, not allowed, nor is any possible radial propagation of "density blobs." Only the radial ion thermal transport and the "heat blob" propagation would be allowed.

Convergence tests in particle number revealed that total of 3.2×10^9 marker particles (average 3500 marker particles per grid node) is adequate for the ITG turbulence study in DIII-D L-mode edge, leaving the noise driven ion thermal transport at the level $\chi_i\simeq0.04$ m^2/s in the studies without ITG generation and collisions. The noise level of χ_i is much lower than the neoclassical χ_i level (~0.2 m^2/s). Convergence test in the grid size shows that we need $\simeq2$ mm average grid size at the outside midplane, which roughly corresponds to ρ_i at the density pedestal shoulder. A usual ITG turbulence simulation with collisions for 1 ms physical time in DIII-D edge takes about 12 h on 14 336 CRAY XT4 cores.

In the collisional turbulence simulation shown here, 2 MW of heat is added at the inner simulation boundary (flat rate at $0.65<\psi_N<0.70$, then linearly decaying to $\psi_N=0.75$) to force the heat flux into the turbulence region. The actual amount of heat flux accepted by the plasma in the beginning of the saturated turbulence stage is only ~1 MW. The leftover heat accumulates to raise T_i in the heating region and $\partial T/\partial r$ in the heating boundary region, gradually increasing the heat flux penetration into the turbulence region. We note here that the heat source region $0.65<\Psi_N<0.75$ is well outside of the physics observation region $\Psi_N>0.85$ and does not affect the self-organized saturation of the plasma temperature profile and turbulence.

Figure 6 shows a two-dimensional electric potential con-

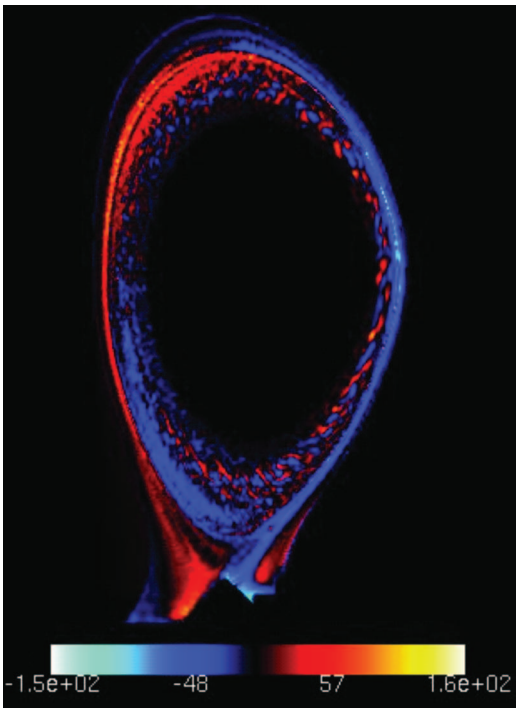

FIG. 6. (Color) Two-dimensional electric potential contour for $\Phi-\Phi_{0,0}$ on a constant toroidal angle plane in the growth stage of edge ITG mode. Poloidally sheared eddies formation is observed across the entire pedestal.

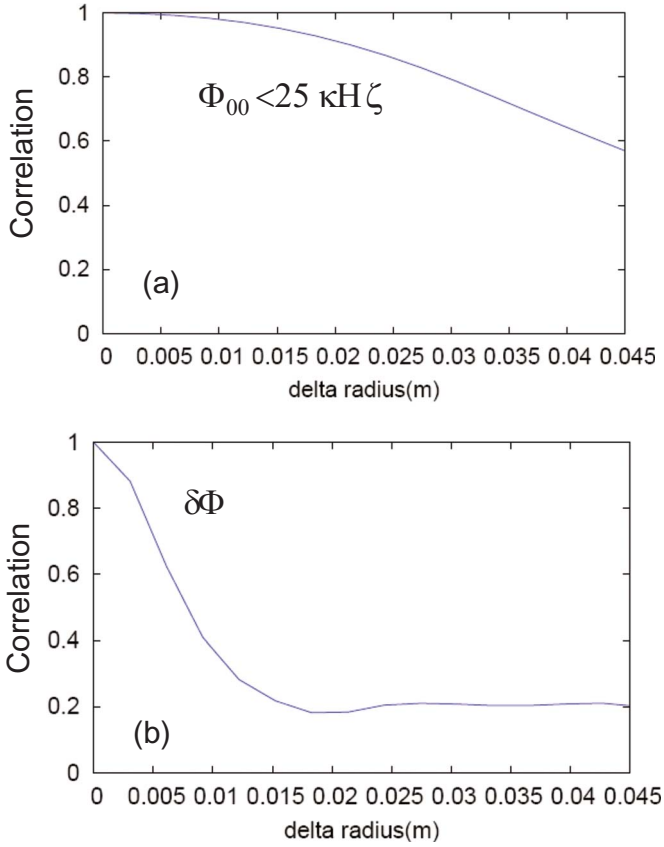

FIG. 7. (Color online) (a) Wide radial correlation of $\Phi_{0,0}$ modes, with greater than 5 cm average correlation length. (b) Radial correlation of the nonaxisymmetric modes, showing about 1 cm average correlation with longer tail.

tour for $\Phi-\Phi_{0,0}$ on a constant toroidal angle plane in the growth stage of ITG modes. Development of eddies, together with the poloidal shearing, can be clearly seen in the edge region. This is in contrast to the radial streamers developed in the linear stage of ITG mode growth in the delta-f core plasma simulations. A close examination reveals that the ITG turbulence eddies form over the whole density pedestal from the top to the bottom.

Also to be noticed in Fig. 6 is the formation of an in-out asymmetry in the electrostatic potential $(\Phi-\Phi_{0,0})/\phi_{0,0}$ on the order of ± 50 eV in the edge plasma. The generation of the in-out asymmetric potential in a conventional tokamak plasma, known to be on the order $[(r/R)\rho_{i\theta}/L_p](q\nu_{ic}/\nu_{it})$, where $\rho_{i\theta}$ is the poloidal ion gyroradius, is negligibly small in a core plasma unless there is a sonic plasma flow, a large impurity flow or other drives.[26–28] However, in the edge plasma considered here, $q(\rho_{i\theta}/L_p)(\nu_{ic}/nu_{it})$ is not small due to the largeness of q and the smallness of L_p, hence the in-out electrostatic potential variation can be non-negligible, as observed in Fig. 6. The safety factor q appearing here is from the long electrical connection distance between the low and high magnetic field sides, while the ion-ion collision frequency ν_{ic} tries to enhance the in-out pressure gradient. A weak up-down asymmetry also exists.

Figure 7(a) shows the wide radial correlation of $\Phi_{0,0}$ modes, with greater than 4.5 cm average correlation length. Figure 7(b) is the radial correlation of the nonaxisymmetric modes, which shows stronger correlation at less than 1 cm together with a significant correlation tail up to >4.5 cm. Considering that the hyperbolic density width is about 4 cm, the nonlocal compressed nature of the turbulence is demonstrated.

In a compressed turbulence, definition of a local thermal conductivity is not well justified due to the nonlocal nature of the turbulence interaction with the equilibrium gradient, as explained earlier. Only the heat flux may be meaningful. However, in order to put the results on a familiar ground, we evaluate an effective local thermal conductivity χ_i by dividing the heat flux by the local temperature gradient. Figure 8(a) shows time behavior of the effective χ_i at the density pedestal top/shoulder and in the middle of the density pedestal slope. The radial locations of the two observation regions are as indicated in Fig. 2(a), with radial average over three grid points. A stronger growth of the ITG-driven effective χ_i can be seen at the top/shoulder than in the slope without an obvious difference in the ITG onset time. However, the effective χ_i at different radial locations converges to a similar level ~ 0.4 m^2/s at later time (which is about one global gyro-Bohm diffusion rate, see Fig. 5, and which is only twice greater than the neoclassical rate $\chi_{i,neo}$ ~ 0.2 m^2/s). The oscillatory behavior is from the GAM activities. Even with the extra preconditioning simulation to remove the spurious GAM growth from local Maxwellian initialization, as explained earlier, we still see the leftover GAM activities in the large-q edge plasma. The GAM amplitude is stronger in the slope region where q is greater (q at the pedestal top/shoulder is about 4.7 and q in the middle of slope is about 5.8). After about nine ion toroidal transit times τ_{it}, we observe that the GAM amplitudes decay (there is a

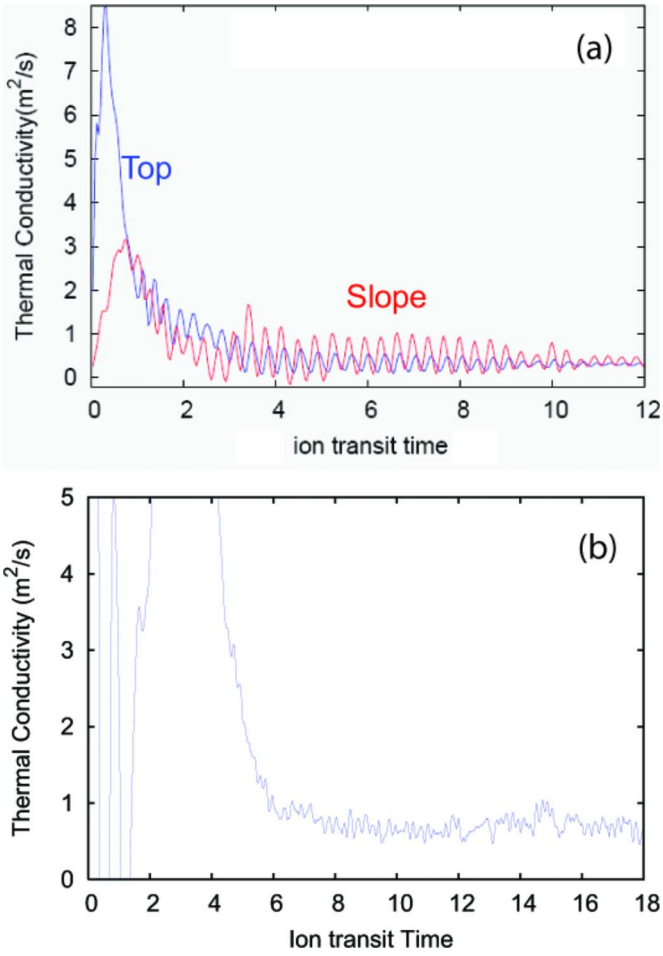

FIG. 8. (Color online) (a) Time behavior of effective χ_i at the top/shoulder and the slope of the density pedestal, with radial averaging over three grid points ($\Delta r \simeq 4$ mm). (b) Time behavior effective χ_i in the core plasma at $q=1.5$. GAM activities are not obvious.

momentary boost at $\sim 10\tau_{it}$ with an unknown cause). Since the GAM oscillation frequency ($\sim$40 kHz) is lower than $\omega_*/2\pi$ in the edge density pedestal slope (see Fig. 4), while GAM frequency is higher than $\omega_*/2\pi$ in the usual core plasma, the effect of reminiscent GAMs on turbulence could be different from the core plasmas, which is unknown at this time. This study is left for a future work. Time evolution of η_i profile is shown in Fig. 3. The blue curve shows the initial η_i profile, the green curve is in the beginning of the nonlinear turbulence plateau ($t=5\tau_{it}$) and the red curve is at the end of the simulation. Most of the changes from the green to red curves occur earlier in the nonlinear plateau phase. In the later phase, η_i stays saturated to the red curve except in the scrape-off region where ion energy is continuously lost to the wall. Reduction in heat input amount by factor of 2 resulted in a similar η_i profile saturation.

For comparison with a conventional low q case, we show the effective χ_i's time behavior from a full-f cyclone core plasma simulation in Fig. 8(b) under a 5 MW of heat source. In this case a preconditioning neoclassical solution has not been used. The wild behavior in the beginning is from the transient neoclassical equilibration process. The local q is 1.5 at the position where χ_i is measured. It can be seen that, unlike the edge case, the GAM activities do not dominate the core χ_i oscillations even though the neoclassical preconditioning is not used. Instead, the thermal transport is close to an avalanche process, as confirmed by $1/f$ type frequency spectrum of χ_i (not shown). When we increase the heating power further in a core simulation, a quasiperiodic intermittent bursty phenomenon dominates the radial thermal transport. These core plasma turbulence behaviors are being reported elsewhere.[29] We have not seen either a clean $1/f$ or bursty behavior in the density slope from the present edge simulation at 2 MW heat source. A heat source scan is planned in the future to examine dependence of edge turbulence and transport characteristics on heating power.

In order to examine further the time behavior of the compressed turbulence in the density slope, a wavelet analysis has been performed. Figure 9 shows the three-dimensional turbulence behavior in time in the wavelet space. The front horizontal axis is the $\log_2$ wavelet scale factor, with the conversion to frequency shown together, and the vertical axis is the wavelet coefficients of the $E\times B$ rotation speed in $\log_{10}$ scale. The other axis is the time, starting from the nonlinear χ_i saturation. Figure 9(a) is at the top/shoulder position and Fig. 9(b) is at the density slope position. For a clearer time behavior of turbulence, Coulomb collisions are turned off in this particular study (collisional damping can mask the zonal flow dynamics[30] and could alter the turbulence behavior). It is seen that there is a more distinctive growth of the zonal flows (around a few to $\sim$10 kHz) in the density slope. It appears, however, that the turbulence itself is generated almost simultaneously in the high η_i region at the density pedestal top/shoulder and in the low η_i region in density slope (Fig. 10). In other words, Fig. 10 does not show an obvious sign of radially outward turbulence front propagation from the pedestal top/shoulder. Instead, it shows a sign of radially inward propagation from the pedestal slope. Normal collisional simulations actually show similar features as the collisionless Fig. 10. Indeed, a whole device simulation with the edge and core together shows a radially inward turbulence front propagation from the pedestal region at a speed $v_s\rho_s/R$.[29] Again in this figure, the residual GAM oscillation is strong at both locations, but its magnitude is stronger in the slope region where q is higher. A likely explanation for the collisionless zonal flow growth in time in the density slope region is the stronger GAM activities, with the inverse cascade of GAM energy into the zonal flows in the absence of collisions.

Another interesting observation made from the present study is the decay of the mean $E\times B$ poloidal rotation speed by ITG turbulence in the edge midplane (Fig. 11, at $\psi_N=0.92$ corresponding to the density pedestal shoulder) while the plasma pressure gradient is relatively fixed in time. We note that the discussion on this subject is speculative at this time and shall be reported in the near future after a more detailed and conclusive study. The ambipolar radial electric field is established quickly within $1\tau_{it}$ (=0.078 ms) from the start of simulation due to the strong neoclassical polarization effect in quasineutral plasma under radial orbital excursions of ions.[3] Once the quasisteady E_r is established, E_r and, thus, the $E\times B$ mean flow in XGC1 does not decay without the

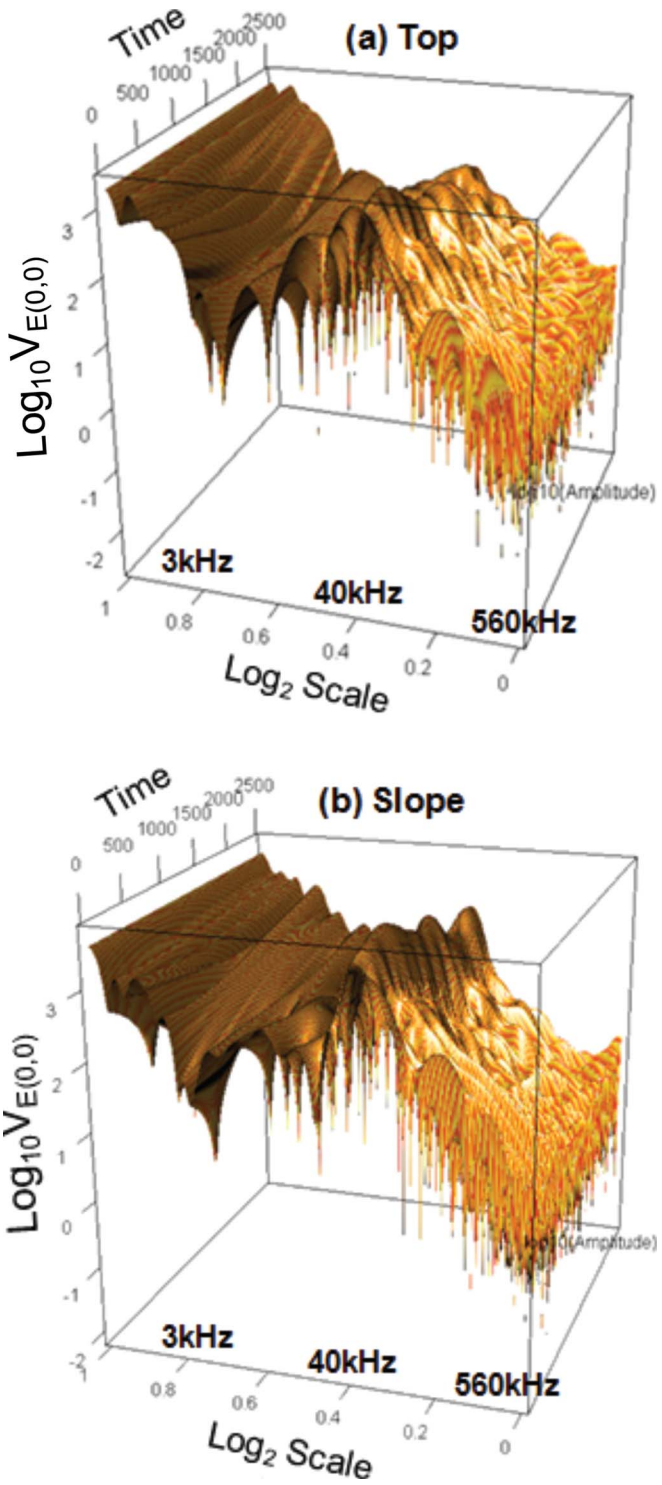

FIG. 9. (Color online) Wavelet analysis of the (0,0) mode behavior without collisions after the nonlinear saturation (a) at the top/shoulder position and (b) in the slope of the density pedestal. The horizontal axes are the log 2 (scale factor) and time. Vertical axis is the log 10 of the wavelet coefficients for the V_{ExB} rotation speed. Conversion of the wavelet scale factor into frequency is shown together.

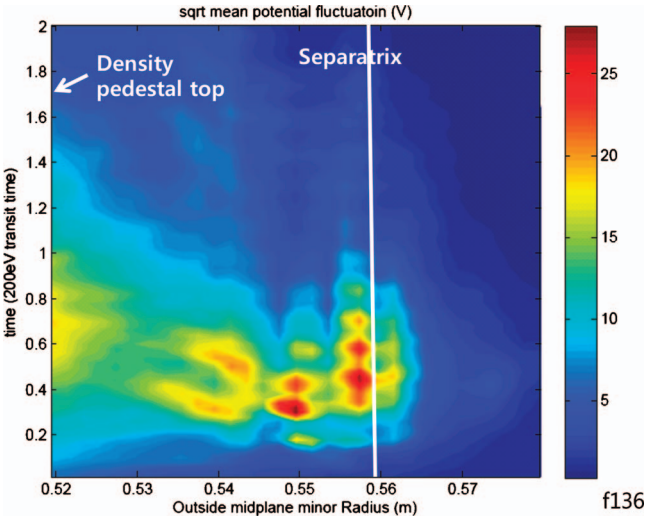

FIG. 10. (Color) Time-radius contour of $\sqrt{(\delta\Phi)^2}$. Radially inward propagation of turbulence front can be noticed.

onset of ITG turbulence.[3] What Fig. 11 shows is a rapid transient neoclassical equilibration process from zero to about $1.5\tau_{it}$, followed by a neoclassical equilibrium between about $1.5-3\tau_{it}$ which would be quasisteady with the turbulence, and another decay after $3\tau_{it}$ with the half decay rate of about 50% of the collision rate. Since this decay rate is on the same order as the collision rate, it is categorized as part of the "mean flow" dynamics as explained earlier. The total simulation time is about two ion-ion collision time, but the decay of E_r has not reached yet to a steady state while the thermal transport already did. Radial profile of the $E\times B$ rotation speeds at $3\tau_{it}$ (where the decay begins) and $12\tau_{it}$ (where simulation ends) is shown in Fig. 12. An overall damping can be seen except very near the magnetic separatrix where the ion X-loss effect is strong, indicating that the ion X-loss effect holds the radial electric field stiff against a possible turbulence effect. During the transient neoclassical equilibration process, however, the E_r profiles in this stiff region changes. A structural difference in E_r profile can also be seen between the strong X-loss region and the radially inside region.

We find that the separatrix and X-loss effects do not change the well-known collisional damping effect of the zonal flows[30] in the edge plasma. Figure 13 is the low-

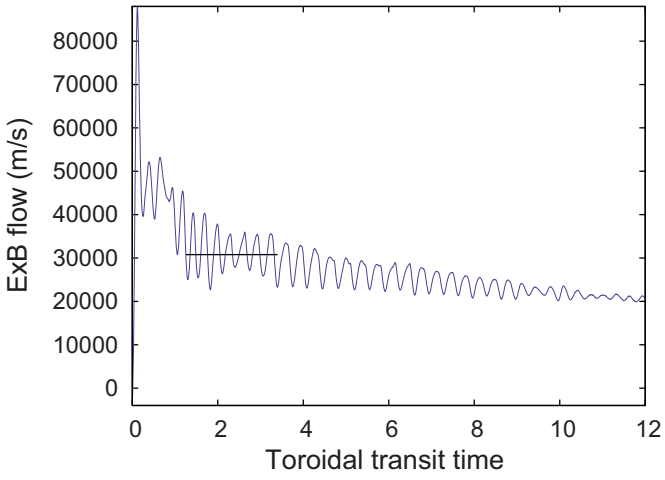

FIG. 11. (Color online) Time behavior of the $E\times B$ rotation during the entire simulation period at the edge density pedestal shoulder (ψ_N=0.92). A line is drawn for visual guide to the neoclassical equilibrium rotation.

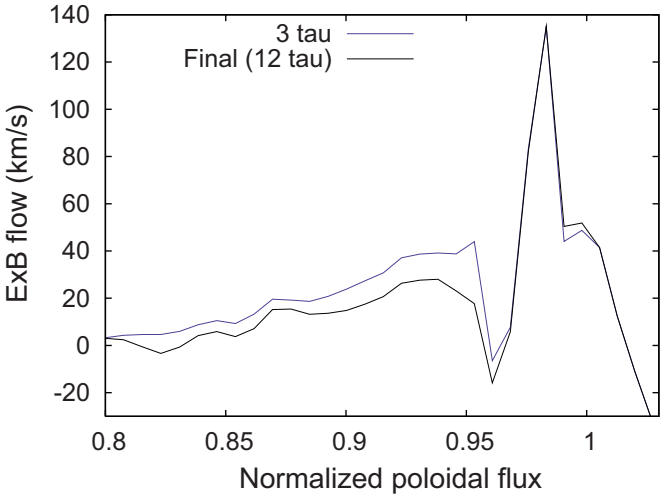

FIG. 12. (Color online) Comparison of the midplane poloidal $E\times B$ rotation profiles at $t=3\tau$ and 12τ. An overall damping can be seen except very near the magnetic separatrix where the ion X-loss effect is strong, indicating that the ion X-loss effect holds the radial electric field constant against a turbulence effect. A structural difference in E_r profile can also be seen between the strong X-loss region and the radially inside region.

frequency wavelet analysis of the (0,0) mode behavior without and with collisions after the nonlinear saturation is achieved. The collisional case (b) shows a significant reduction in the zonal flows, when compared to the collisionless case (a). Figure 14 displays the edge turbulence spectrum in $k_\theta\rho_i$ for the two cases, which is consistent with the collisional zonal flow damping.

V. CONCLUSIONS AND DISCUSSIONS

The full-f gyrokinetic particle code XGC1 has been used to study the ITG turbulence in a realistic geometry diverted tokamak edge. Turbulent and neoclassical physics are simulated together. A heat source is introduced at the inner boundary to induce a finite heat flux into the turbulence simulation region. Electrostatic potential at the material wall is grounded to zero and the radial electric field at the turbulence-free inner boundary (core-edge boundary) is set to zero. Particle-momentum-energy conserving Monte Carlo collision operator is used.

It is found that there is a radially compressed ITG turbulence across the entire L-mode edge density pedestal in diverted tokamak geometry, in which a mild ion temperature gradient makes the normalized ion temperature gradient parameter $\eta_i=(d\log T_i/dr)/(d\log n/dr)$ to vary strongly from high (>4 at density top/shoulder) to low (<2 in the slope) values. The growth of the turbulence appears to be simultaneous across the edge region. The resulting heat flux in a pure deuteron plasma is on the order of experimentally inferred value and shows a broad and mild radial variation in spite of the rapid η_i variation. Particularly, the ITG turbulence and the heat flux exist in the density slope region where η_i is much below the critical level estimated from idealized linear ITG stability theories. Thus, the present study strongly suggests that a localize estimate of the ITG-driven χ_i will not be valid due to the nonlocal dynamics of

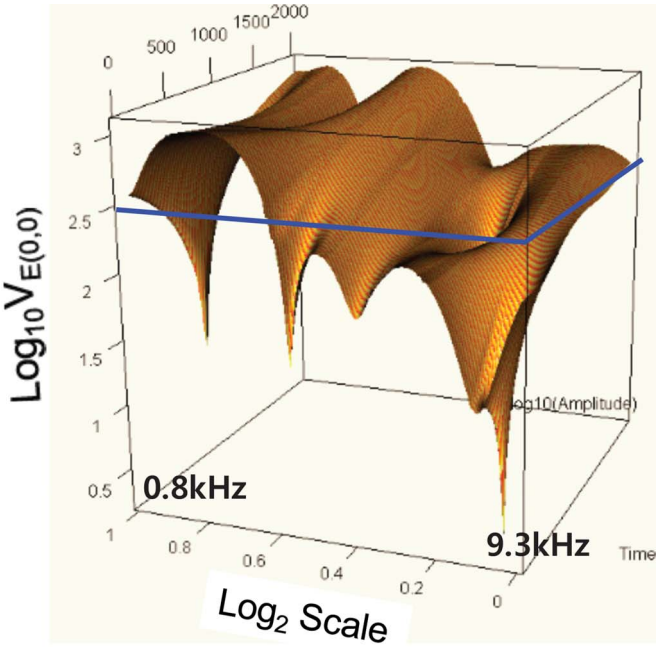

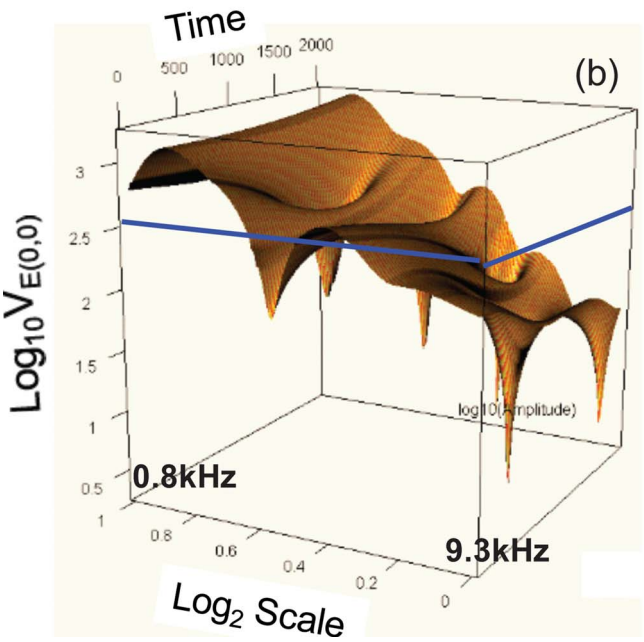

FIG. 13. (Color online) Low frequency wavelet analysis of the (0,0) zonal flow behaviors (a) without collisions and (b) with collisions in the density slope after the nonlinear saturation. Conversion of the wavelet scale factor into frequency is shown together. A significant collisional reduction of the zonal flow amplitude can be seen.

the compressed turbulence in an L-mode density pedestal. The distance between the linearly stable and unstable regions (as conventionally defined) is within the turbulence correlation length.

Turbulence characteristics observed in the edge density slope are different from the usual delta-f core turbulence characteristics. In addition to the compressed nature of the turbulence, there is a strong interaction with the mean plasma from the beginning. In other words, the usual linear growth stage is not seen, in which the radially elongated

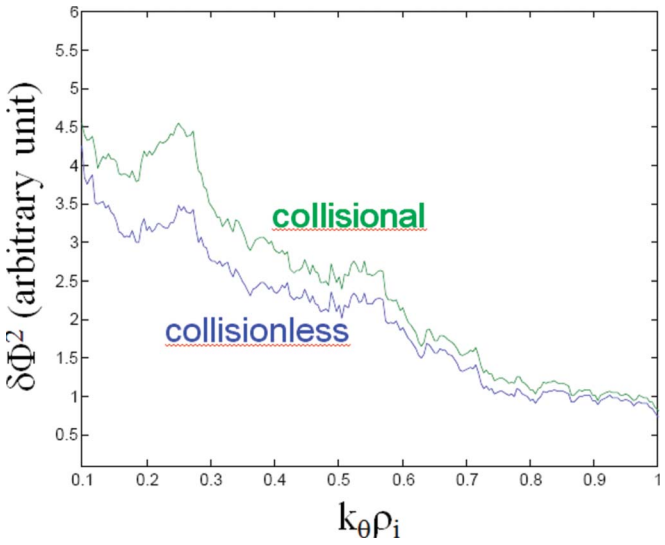

FIG. 14. (Color online) Spectrum of the fluctuating turbulence energy in $k_\theta\rho_i$.

streamers would grow. Instead, the growth of ITG turbulence starts with turbulent eddies with poloidally sheared structures caused by interaction with the mean flow shears. The thermal transport and background ion temperature profiles evolve to a self-organized state. The background $E\times B$ flow damps, but at a slower rate than the thermal transport and temperature profile saturation rates.

The results reported here are mostly "observational." More detailed quantitative studies will be reported elsewhere in the near future. Kinetic electron effect on plasma turbulence and particle transport has not been studied yet in XGC1, and to be pursued in the future with high priority.

ACKNOWLEDGMENTS

XGC1 full-f gyrokinetic code has been developed collaboratively in the SciDAC FSP Prototype Center for Plasma Edge Simulation (CPES). The authors wish to express special acknowledgment to the performance engineering, applied mathematics, and data management team members for their invaluable contribution to the XGC code development. One of the authors (C.S.C.) acknowledges helpful discussions with W. W. Lee and G. Hammett of PPPL. We also acknowledge that XGC1 adopted the basic features of the single particle motions from the ORBIT code[31] and many of the global delta-f gyrokinetic simulation techniques from the core turbulence gyrokinetic toroidal code GTC,[32] even though the coordinate systems and the magnetic topology are different.

This research has been funded by U.S. Department of Energy, jointly between the Office of Fusion Energy Science and the Office of Advanced Scientific Computing Research, and Korean ERC and KSTAR fusion programs. The computation was made possible through the INCITE award on NCCS Jaguar, "Verification and validation of petascale simulation of turbulent transport in fusion plasmas," and a generous ERCAP computing support at NERSC Franklin.

[1] R. Aymar, V. A. Chuyanov, M. Huguet, Y. Shimomura, and ITER Joint Central Team and ITER Home Teams, Nucl. Fusion **41**, 1301 (2001).
[2] R. J. Groebner, K. H. Burrell, and R. P. Seraydarian, Phys. Rev. Lett. **64**, 3015 (1990); M. Greenwald, R. L. Boivin, F. Bombarda, P. T. Bonoli, C. L. Fiore, D. Garnier, J. A. Goetz, S. N. Golovato, M. A. Graf, R. S. Granetz, S. Horne, A. Hubbard, I. H. Hutchinson, J. H. Irby, B. LaBombard, B. Lipschultz, E. S. Marmar, M. J. May, G. M. McCracken, P. O'Shea, J. E. Rice, J. Schachter, J. A. Snipes, P. C. Stek, Y. Takase, J. L. Terry, Y. Wang, R. Watterson, B. Welch, and S. M. Wolfe, Nucl. Fusion **37**, 793 (1997).
[3] C. S. Chang and S. Ku, Phys. Plasmas **15**, 062510 (2008).
[4] S. Ku, C. S. Chang, M. Adams, J. Cummings, F. Hinton, D. Keyes, S. Klasky, W. Lee, Z. Lin, S. Parker, and the CPES team, J. Phys.: Conf. Ser. **46**, 87 (2006).
[5] J. L. Luxon, Nucl. Fusion **42**, 614 (2002).
[6] W. W. Lee, Phys. Fluids **26**, 556 (1983).
[7] J. A. Heikkinen, S. Henriksson, S. Janhunen, T. P. Kiviniemi, and F. Ogando, Contrib. Plasma Phys. **46**, 490 (2006).
[8] X. Garbet, Y. Sarazin, V. Grandgirard, G. Dif-Pradalier, G. Darmet, Ph. Ghendrih, P. Angelino, P. Bertrand, N. Besse, E. Gravier, P. Morel, E. Sonnendrucker, N. Crouseilles, J.-M. Dischler, G. Latu, E. Violard, M. Brunetti, S. Brunner, X. Lapillonne, T.-M. Tran, L. Villard, and M. Boulet, Nucl. Fusion **47**, 1206 (2007).
[9] Y. Idomura, M. Ida, T. Kano, N. Aiba, and S. Tokuda, Comput. Phys. Commun. **179**, 391 (2008).
[10] C. S. Chang and S. Ku, Phys. Plasmas **11**, 2649 (2004).
[11] C. S. Chang and S. Ku, Contrib. Plasma Phys. **46**, 496 (2006).
[12] R. White, Phys. Fluids B **2**, 845 (1990); A. H. Boozer, Phys. Fluids **27**, 2441 (1984); R. G. Littlejohn, *ibid.* **28**, 2015 (1985).
[13] Y. Nishimura, Z. Lin, J. L. V. Lewandowski, and S. Ethier, J. Comput. Phys. **214**, 657 (2006); Y. Idomura, S. Tokuda, and Y. Kishimoto, J. Plasma Fusion Res. **6**, 17 (2004).
[14] Z. Lin and W. Lee, Phys. Rev. E **52**, 5646 (1995).
[15] L. L. Lao, H. St. John, R. D. Stambaugh, A. G. Kellman, and W. Pheiffer, Nucl. Fusion **25**, 1611 (1985).
[16] W. X. Wang, N. Nakajima, M. Okamoto, and S. Murakami, Plasma Phys. Controlled Fusion **41**, 1091 (1999); X. Q. Xu and M. N. Rosenbluth, Phys. Fluids B **3**, 627 (1991); A. M. Dimits and B. I. Cohen, Phys. Rev. E **49**, 709 (1994); Z. Lin, W. M. Tang, and W. W. Lee, Phys. Plasmas **2**, 2975 (1995).
[17] P. Diamond, S.-I. Itoh, K. Itoh, and T. S. Hahm, Plasma Phys. Controlled Fusion **47**, R35 (2005).
[18] H. Biglari, P. H. Diamond, and P. Terry, Phys. Fluids B **2**, 1 (1990).
[19] E. Kim and P. H. Diamond, Phys. Rev. Lett. **90**, 185006 (2003).
[20] H. Biglari, P. H. Diamond, and M. N. Rosenbluth, Phys. Fluids B **1**, 109 (1989).
[21] W. Horton, Rev. Mod. Phys. **71**, 735 (1999).
[22] R. D. Hazeltine and J. D. Meiss, *Plasma Confinement*, Frontiers in Physics (Addison-Wesley, Redwood City, CA, 1992), p. 367.
[23] Y. Idomura, S. Tokuda, and Y. Kishimoto, Nucl. Fusion **43**, 234 (2003).
[24] P. Angelino, A. Bottino, R. Hatzky, S. Jolliet, O. Sauter, T. M. Tran, and L. Villard, Phys. Plasmas **13**, 052304 (2006).
[25] G. Dif-pradalier, V. Grandgirard, Y. Sarazin, X. Garbet, Ph. Ghendrih, and P. Angelino, Phys. Plasmas **15**, 042315 (2008).
[26] C. S. Chang and R. D. Hazeltine, Nucl. Fusion **20**, 1397 (1980); Phys. Fluids **25**, 538 (1982).
[27] C. S. Chang and R. W. Harvey, Nucl. Fusion **23**, 935 (1983).
[28] C. S. Chang, Phys. Fluids **26**, 2140 (1983).
[29] S. Ku, C. S. Chang, and P. H. Diamond, "Full-f gyrokinetic particle simulation of ITG turbulence with a strong central heating in realistic tokamak geometry," Nucl. Fusion (to be published).
[30] F. L. Hinton and M. N. Rosenbluth, Plasma Phys. Controlled Fusion **41**, A653 (1999).
[31] R. B. White and M. S. Chance, Phys. Fluids **27**, 2455 (1984).
[32] Z. Lin, T. S. Hahm, W. W. Lee, W. M. Tang, and R. B. White, Science **281**, 1835 (1998).